JOURNAL OF GEOPHYSICAL RESEARCH, VOL. 105, NO. B7, PAGES 16,229–16,236, JULY 10, 2000

Strain accumulation across the Eastern California Shear Zone at latitude 36°30'N

Weijun Gan,[1] J. L. Svarc, J. C. Savage, and W. H. Prescott

U.S. Geological Survey, Menlo Park, California

Abstract. The motion of a linear array of monuments extending across the Eastern California Shear Zone (ECSZ) has been measured from 1994 to 1999 with the Global Positioning System. The linear array is oriented N54°E, perpendicular to the tangent to the local small circle drawn about the Pacific-North America pole of rotation, and the observed motion across the ECSZ is approximated by differential rotation about that pole. The observations suggest uniform deformation within the ECSZ (strike N23°W) (26 nstrain yr^{-1} extension normal to the zone and 39 nstrain yr^{-1} simple right-lateral shear across it) with no significant deformation in the two blocks (the Sierra Nevada mountains and southern Nevada) on either side. The deformation may be imposed by right-lateral slip at depth on the individual major fault systems within the zone if the slip rates are: Death Valley-Furnace Creek fault 3.2±0.9 mm yr^{-1}, Hunter Mountain-Panamint Valley fault 3.3±1.6 mm yr^{-1}, and Owens Valley fault 6.9±1.6 mm yr^{-1}. However, this estimate of the slip rate on the Owens Valley fault is 3 times greater than the geologic estimate.

1. Introduction

The Eastern California Shear Zone (ECSZ) [*Dokka and Travis*, 1990a,b] is a ~100-km-wide zone of deformation trending north-northwest into Nevada from the east end of the "big bend" in the San Andreas fault (Figure 1). North of the Garlock fault the ECSZ spans the Owens Valley-Little Lake, Hunter Mountain-Panamint Valley, and Death Valley-Furnace Creek-Southern Death Valley fault systems (Figure 2). The 1992 M=7.5 Landers earthquake occurred near the southern end of the ECSZ and the 1872 M=7.6 Owens Valley earthquake occurred near its northern end (Figure 1). The shear zone accommodates ~24% of the Pacific-North American relative plate motion (M.M. Miller et al., Refined kinematics of the Eastern Californua Shear Zone from GPS observations, 1983-1998, submitted to *Journal of Geophysical Research*, 2000; hereinafter referred to as Miller et al., submitted manuscript). As is the case for other zones of distributed deformation [*Savage et al.*, 1999a], it is not clear whether the deformation in the zone is simply a manifestation of strain accumulation due to slip at depth on closely spaced faults within the zone or is imposed by drag from a continuous distribution of deformation in the viscous upper mantle [*Bourne et al.*, 1998]. The former explanation implies that the strength of the lithosphere resides principally in the upper crust, whereas the latter explanation implies that it resides in the upper mantle.

To study the distribution of deformation across the ECSZ the U.S. Geological Survey in late 1994 installed a linear array of geodetic monuments (shear zone array in Figure 2) along an azimuth of about N54°E extending from the Sierra Nevada mountains to near Beatty, Nevada. The array was surveyed in 1994, 1996, 1997, and 1999 using the Global Positioning System (GPS). That array of monuments joined another geodetic strain array (Yucca Mountain array in Figure 2) centered on Yucca Mountain, Nevada, which had been surveyed in 1993 and 1998 using GPS [*Savage et al.*, 1999b]. Before 1995, codeless Ashtech LM-XII GPS receivers were used. Resolution of phase ambiguities was difficult in those surveys. By 1995 the receivers had been upgraded to Ashtech Z-12's, which receive full-wavelength data and allowed better resolution of phase ambiguities. In the 1994 survey of the shear zone array the individual monuments in the array were occupied for at least 6 hours in each survey; in the other surveys the occupations were with few exceptions for 6 or more hours on each of two or more consecutive days (see the Web locations cited below for occupation histories). The data were reduced using point positioning [*Zumberge et al.*, 1997] and GIPSY/OASIS-II software, release 5 [*Webb and Zumberge*, 1995]. The solutions are referred to the International Terrestrial Reference Frame 1996 (ITRF96) [*Sillard et al.*, 1998] rotated so that North America is nominally fixed [*Savage et al.*, 2000, appendix] (i.e., the rotation is determined so as to minimize the velocities at the fiducial stations Algo (Ontario, Canada), Brmu (Bermuda), Drao (British Columbia, Canada), Fair (Alaska), Nlib (Iowa), Piel (New Mexico), and Yell (Northwest Territories, Canada)). Because it is not certain that all of the fiducial stations are in fact fixed with respect to North America, the velocities relative to fixed North America assigned to the monuments in the array discussed here have a common (systematic) uncertainty of perhaps one or two millimeters per year. The relative velocities of the monuments within the array, however, are free of that systematic error.

The overall accuracy in locating one geodetic monument with respect to another out to 400 km was expected to be ~4 mm (one standard deviation) in each horizontal component [*Zhang et al.*, 1997] for a daily solution. However, in this paper the error estimates, determined by scaling upward the formal errors from the solution by a factor found appropriate

[1] On leave from the Institute of Geology, China Seismological Bureau, Beijing.

Paper number 2000JB900105.

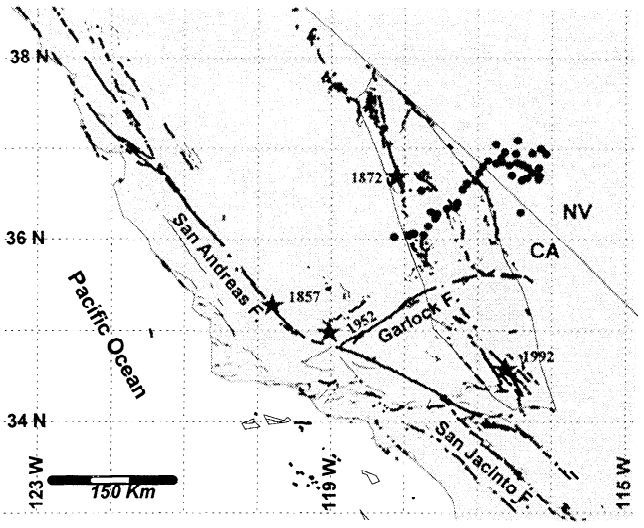

Figure 1. Map showing the principal faults in southern California and the location of the Eastern California Shear Zone (shaded). The locations of the monuments in the geodetic array are shown by solid dots. Epicenters of the 1857 Fort Tejon,1872 Owens Valley, 1952 Kern County, and 1992 Landers earthquakes are shown by stars.

from the linear fits to displacement versus time plots of individual stations [*Savage et al.*, 2000, p. 3102], are somewhat greater (see error bars in Figure 3), particularly in the early surveys. The additional uncertainty may be due to monument instability but more likely simply reflects the uncertainty in locating monuments with respect to the more distant fixed interior of North America. This estimated uncertainty does not include the systematic error in fixing the reference frame with respect to stable North America. An independent estimate of the standard deviation of the velocities for the Yucca Mountain array (abscissa >20 km in Figure 4) based on the assumption that there is no significant relative motion between monuments in that array is consistent with the standard deviations used here (J.C. Savage et al., Strain accumulation near Yucca Mountain, Nevada, 1993-1998, submitted to *Journal of Geophysical Research*, 2000).

In this paper we adopt the following conventions: All uncertainties quoted in the text and tables are standard deviations, but the error bars in the figures extend 2 standard deviations on either side of the plotted points. In discussing strain, extension is reckoned positive.

2. Data

Detailed data (latitude and longitude of the monuments, positions of monuments as a function of time, and velocities inferred for the monuments) and plots for the two arrays are available on the Web at http://quake.wr.usgs.gov:80/QUAKES/geodetic/gps/Yucca.qoca/. That Web site will be updated as new data become available.

The observed changes in monument positions in a reference frame nominally fixed with respect to the interior of the North American plate are shown in Figure 3 as a function of time for those monuments occupied in more than two surveys. (See the Web site referenced above for plots of all data. Only two monuments, 1pdi and Shos, in the Yucca Mountain array were occupied in more than two surveys and thus are the only monuments from the Yucca Mountain array shown in Figure 3.) In Figure 3 the displacements from arbitrary positions fixed in our reference frame have been resolved into N36°W (direction of the tangent to the local small circle drawn about the Pacific-North American pole of motion [*DeMets et al.*, 1990]) and N54°E components. A straight line, the slope of which represents the monument velocity relative to the reference frame, has been fit to the observed displacements at each station. The data in Figure 3 are reasonably well explained by the linear fits. Thus we assume that the motion of the monuments has been uniform in time. On the basis of that assumption we have used the adjustment program QOCA [*Dong et al*, 1998] (see also the Web site http://sideshow.jpl.nasa.gov:80/~dong/qoca/) in the global mode to find the velocity at each monument (Figure 2).

The velocity at monument Go05 is clearly anomalous (Figure 2). That monument is close to the Coso geothermal field and also to the epicenters (Figure 2) of three magnitude 5 earthquakes which occurred in 1996 and 1998 [*Bhattacharyya et al.*, 1999], within the interval of observation. R.W. King (personal communication, 2000), who has analyzed detailed GPS surveys in the vicinity of the geothermal area, does not believe that the earthquakes near Coso had any significant effect on GPS stations in our array. *Wicks et al.* [1999] report 1992-1997 subsidence at the rate of 30 mm yr^{-1} centered on the geothermal area at Coso; the subsidence is reasonably well modeled by the collapse of a spherical source (cross in Figure 2) at a depth of 3.5 km. Because the subsidence probably affected Go05, we will exclude that monument from further discussion in this paper. Monuments Fork and V511 may also be affected by the deformation in the Coso geothermal field, but we retain those monuments in this discussion.

The velocities determined from the QOCA adjustment are plotted in Figure 4 as functions of the distance in the N54°E direction from monument Mo93 on the California-Nevada state line. The velocities have been resolved into N54°E and N36°W components, perpendicular and parallel, respectively, to the tangent to the local small circle drawn about the Pacific-North American pole of rotation. The N54°E velocity component (Figure 4b) indicates little systematic motion in that direction. The profile for the N36°W velocity component (Figure 4a) suggests shear across the tangent to the small circle, but that shear is confined entirely to the monuments in California (negative abscissa in Figure 4). The California-Nevada state line seems roughly to coincide with the eastern edge of the shear zone at this latitude.

3. Strain Analysis

Figure 4 suggests that deformation in California (negative abscissa in Figure 4) is relatively uniform, whereas deformation in Nevada (positive abscissa in Figure 4) is negligible. To examine this further we have solved for the uniform strain that best approximates the observed deformation in California and Nevada separately. The QOCA adjustment program outputs the uniform strain rate and rigid body motion most consistent with the velocity solution for any subset of the adjusted array. We have chosen to examine two subarrays, one composed of the monuments in California and the other composed of the monuments in Nevada.

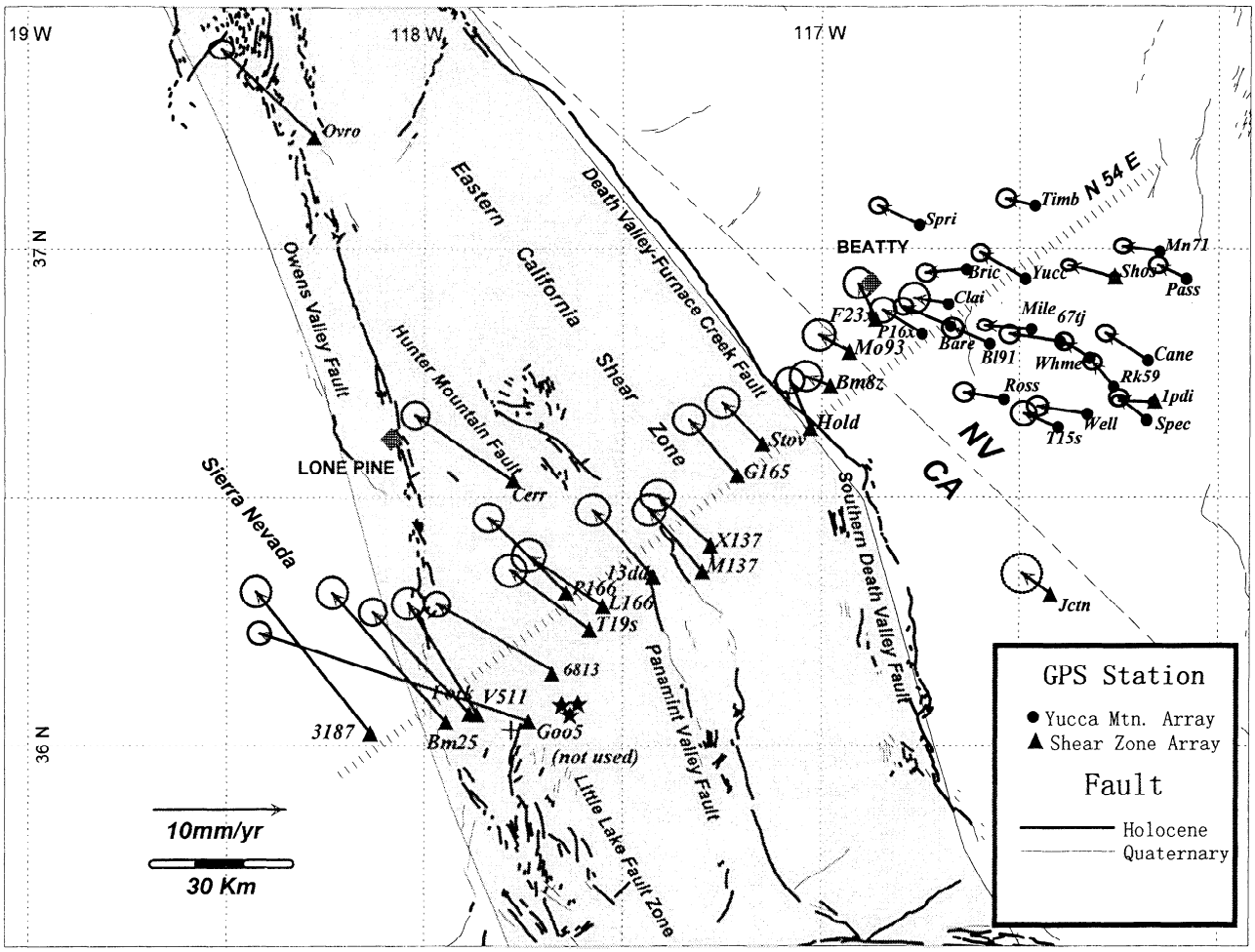

Figure 2. Map of the GPS arrays across the Eastern California Shear Zone (solid triangles) and around Yucca Mountain (solid circles). The velocity relative to the fixed interior of North America for each monument is shown by an arrow. The 95% confidence ellipse is shown at the tip of the arrow. The locations of the towns Beatty, Nevada, and Lone Pine, California, are shown as shaded diamonds. The principal faults are shown by sinuous black lines, and the California-Nevada state boundary is shown by the diagonal dashed line across the figure. The diagonal hachured line trends N54°E, perpendicular to the tangent to the local small circle drawn about the Pacific-North American pole of rotation. The epicenters of the three magnitude 5 earthquakes in 1996 and 1998 that occurred 15 km east of the Coso geothermal field are shown by the stars and the center of the spherical source used by *Wicks et al.* [1999] to model the subsidence in the Coso Geothermal area is shown by the nearby cross.

Monument Mo93, located on the state line, is assigned to the Nevada subarray. The principal strain rates and the rotation rates found for those two subarrays are shown in Table 1. From independent Geodolite measurements of the 30-km-wide Owens Valley trilateration network, which extends between monuments Cerr and Ovro (Figure 2), *Savage and Lisowski* [1995] found that the principal strain rates for the western portion of the ECSZ (Owens Valley) were 82±15 nstrain yr^{-1} N73°±3°W and -39±15 nstrain yr^{-1} N17°±3°E, extension reckoned positive. Although that strain rate is consistent at the 2-st.d. level with the strain rate for the California subarray in Table 1, the Owens Valley strain rates do nevertheless suggest that strain accumulation in the western part of the California subarray (Owens Valley) may be higher than the average rate over the entire subarray (Table 1).

As suggested by Figure 4 the strain rates for the California subarray (Table 1) can be approximated by simple shear across vertical planes parallel to the tangent to the local small circle drawn about the North American-Pacific pole of rotation. In a coordinate system with the 2 axis directed N36°W parallel to that tangent the strain rates are $\dot{\varepsilon}_{11}$= 6.7±6.5 nstrain yr^{-1}, $\dot{\varepsilon}_{12}$= -40.7±4.4 nstrain yr^{-1}, and $\dot{\varepsilon}_{22}$= 18.2±7.2 nstrain yr^{-1}. In this case $\dot{\varepsilon}_{11}$ is not significant, $\dot{\varepsilon}_{22}$ is only marginally significant, and $\dot{\varepsilon}_{12}$ differs significantly from the rotation rate ω (Table 1) only in sign (i.e., $\dot{\varepsilon}_{12}$=-ω). Thus, to a reasonable approximation the deformation field represents simple ($\dot{\varepsilon}_{12}$=-ω) shear across vertical planes parallel to the tangent to the local small circle. That is, the motion across the shear zone is approximated by rotation about the Pacific-North American pole of rotation with angular velocity increasing with distance from the pole.

An interpretation of the California subarray strain rates somewhat more consistent with the simple shear is suggested by a resolution of the strain field in a coordinate system with

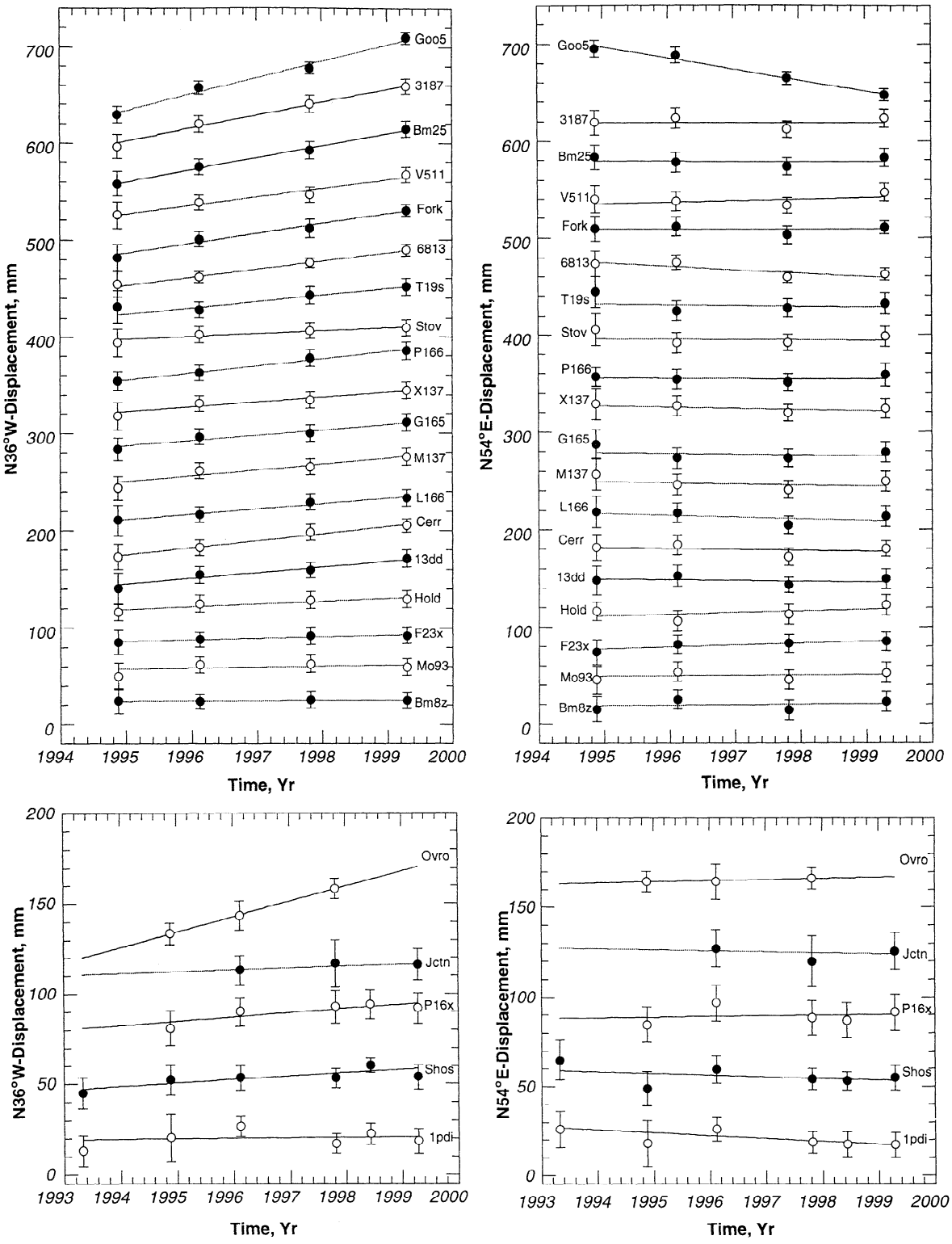

Figure 3. Plots of displacement referred to an arbitrary origin as a function of time for all monuments in the geodetic arrays measured in more than two surveys. The displacements have been resolved into N36°W and N54°E components. The error bars represent two standard deviations on either side of the plotted point.

the 2 axis parallel to the N23°W trend of the ECSZ. In that coordinate system the strain rates are $\dot{\varepsilon}'_{11}$= 24.9±6.5 nstrain yr^{-1}, $\dot{\varepsilon}'_{12}$= -39.2±4.4 nstrain yr^{-1}, and $\dot{\varepsilon}'_{22}$= 0.0±7.2 nstrain yr^{-1}. Notice that the shear rate $\dot{\varepsilon}'_{12}$ differs significantly from the rotation rate ω (Table 1) only in sign (i.e., $\dot{\varepsilon}'_{12}$=-ω) and the extension rate $\dot{\varepsilon}'_{22}$ parallel to the trend of the shear zone is negligible. Our preferred interpretation of deformation in the ECSZ at this latitude is simple shear across the trend of the zone plus extension perpendicular to it.

The deformation of the Nevada subarray (Table 1) is at best

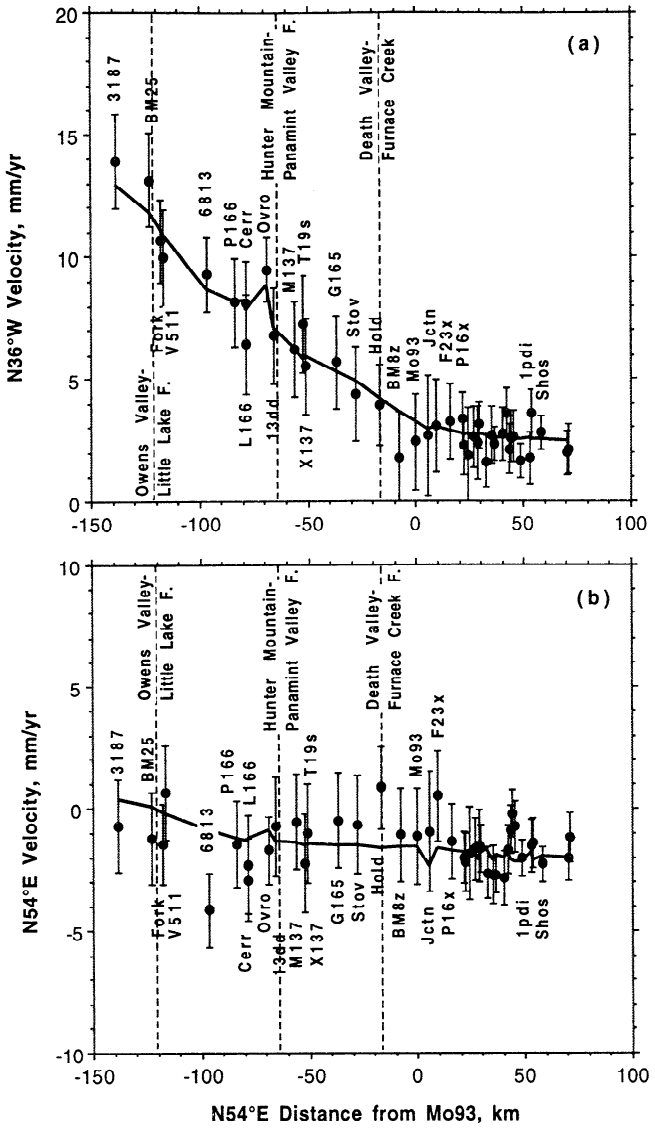

Figure 4. Profiles of the (a) N36°W and (b) N54°E components of velocity as a funcition of distance N54°E from monument Mo93 on the California-Nevada boundary. The error bars represent two standard deviations on either side of the plotted point. The continuous solid lines indicate the velocites predicted by the dislocation model of Table 2. The dashed vertical lines indicate the location of profile crossings of the principal faults.

marginally significant [*Savage et al.*, 1999b]. *Wernicke et al.* [1998] have argued that independent GPS surveys of monuments Clai, Bl91, Mile, 67tj and Whme (Figure 2) from 1991 to 1998 indicate a N65°W strain rate of 50±8 nstrain yr^{-1}. However, the data available to *Wernicke et al.* [1998] were much less complete than the U.S. Geological Survey data used here, and we are confident that the strain rate in the Nevada subarray is very low (Table 1). The observed absence of significant strain accumulation in the Nevada subarray is of some importance as the proposed U. S. high-level radioactive waste disposal repository is located close to monument Mile (Figure 2).

The observed deformation of the entire geodetic array (California plus Nevada subarrays) can be represented by a flat-Earth model in which the relative motion between two rigid plates is accommodated by uniform deformation in the parallel-sided zone that separates them [*Savage et al.*, 1995, appendix]. That is, the curvature of the Earth is neglected and southern Nevada and the Sierra Nevada mountains are represented by rigid blocks separated by a parallel-sided zone (ECSZ) subject to uniform deformation (Figure 5b). We have shown above that the strain rate in the Nevada subarray to the east of the shear zone is not significant, and the Sierra Nevada block to the west of the shear zone is generally treated as rigid [e.g., *Hearn and Humphreys*, 1998]. Thus approximating the Sierra Nevada block and the southern Nevada block as rigid plates is reasonable. The strain within the ECSZ (California subarray) conforms to the requirements ($\dot{\varepsilon}_{12}=-\omega$ and $\dot{\varepsilon}_{22}=0$) for a zone of deformation separating two rigid plates [*Savage et al.*, 1995, appendix] (notice that in this reference the sign convention for ω is opposite that employed here). Thus the ECSZ can be interpreted [*Savage et al.*, 1995, appendix] as a zone of uniform deformation separating rigid plates (southern Nevada and the Sierra Nevada mountains). Notice that in this flat-Earth model, there is no rotation of the Sierra Nevada plate relative to southern Nevada. Specifically, there is no apparent rotation of the Sierra Nevada block relative to fixed interior North America that would permit a fan-like opening of the Basin and Range province to accommodate more east-west spreading in the north than in the south [*Bogen and Schweickert*, 1985]. Nor was such a rotation found in the preferred representation (model M2) of deformation in the same area by *Hearn and Humphreys* [1998].

4. Fault Model

Here we attempt to explain the deformation observed across the ECSZ as being generated by strike slip at depth on the three principal fault systems (the Death Valley-Furnace Creek, the Hunter Mountain-Panamint Valley, and the Owens Valley-Little Lake) that cross the geodetic array (fault crossings are indicated by vertical dashed lines in Figure 4). We have represented the fault systems by simple dislocations in an elastic half-space [*Okada*, 1985] and determined the Burgers vector for each dislocation such that the observed velocity field is best explained. The faults are represented by dislocation segments as shown in Figure 5a. The Owens Valley-Little Lake fault system has been represented by a single screw dislocation and the Death Valley-Furnace Creek-Southern Death Valley and Hunter Mountain-Panamint Valley fault systems have each been represented by segmented screw dislocations. All dislocations are placed at a depth of 15 km (the locking depth), and the slip on each fault system is constrained to be constant along the length of the system (e.g., slip on the Hunter Mountain fault is the same as on the Panamint Valley fault). Notice that no allowance has been made for normal slip on the Death Valley-Furnace Creek-Southern Death Valley and Hunter Mountain-Panamint Valley fault systems nor on the Sierra frontal fault system, although such slip probably occurs there; data on vertical deformation would be required to effectively constrain such normal slip. The best fit values for slip rates on the various fault systems are shown in Table 2. With the important exception of the 2 mm yr^{-1} geologic slip rate estimate for the Owens Valley fault [*Beanland and Clark*, 1994], the slip rates in Table 2 are within the range of previous geologic and geodetic estimates

Table 1. Uniform Principal Strain and Rotation Rate Approximations to Observed Deformation in the Subarrays

Subarray	$\dot{\varepsilon}_1$, nstrain yr^{-1}	$\dot{\varepsilon}_2$, nstrain yr^{-1}	ω, nrad. yr^{-1}
California	53.6±6.9 N77°± 3W	-28.7±5.5 N13°± 3°E	37.1±4.1
Nevada	9.9±5.4 N60°±13°E	-11.5±7.4 N30°±13°E	6.0±4.4

Quoted uncertainties are standard deviations

(see Table 1 of *Hearn and Humphreys* [1998] for a recent compilation of slip rates) and reproduce the observed deformation satisfactorily (continuous lines in Figure 4). Moreover, the slip rate estimates in Table 2 are completely consistent with similar estimates of *Bennett et al.* [1997], *McClusky et al.* [1999], and Miller et al. (submitted manuscript, 2000) based on independent GPS measurements. However, because the velocity profiles across the shear zone are relatively smooth, our dislocation models for the individual faults are not closely defined. For example, changing the locking depth to 10 or 20 km does not change the slip rates significantly and gives almost as good a fit to the observations as the 15 km locking depth employed.

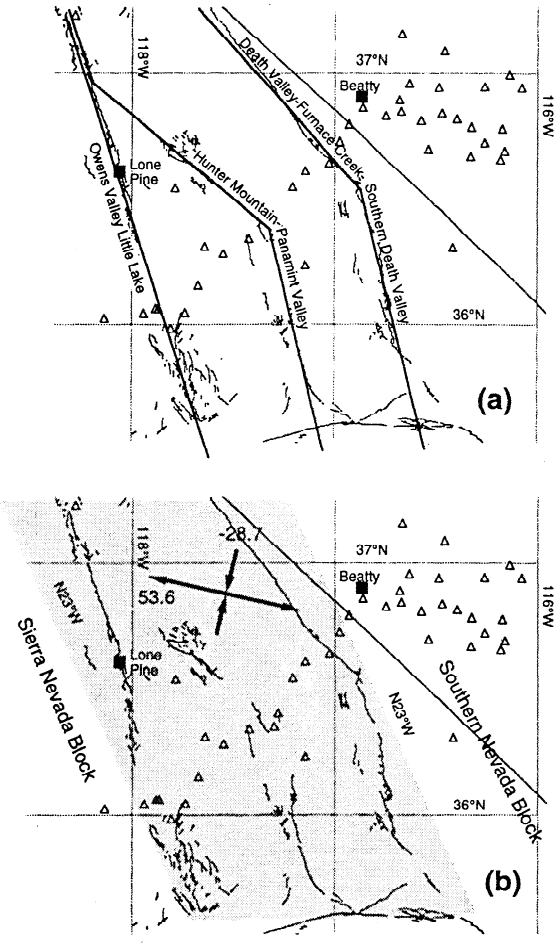

Figure 5. Two models of deformation in the ECSZ. (a) Deformation attributed to slip at depth on individual faults. The traces of the dislocation slip planes used to represent the three major fault systems are shown by the heavy straight lines. (b) Deformation attributed to uniform strain accumulation (heavy crossed arrows with principal strain rates in nanostrain per year) in a parallel-sided shear zone (shaded) with no strain accumulation in the blocks on either side of it.

The discrepancy between the geologic estimate of slip rate (2±1 mm yr^{-1} [*Beanland and Clark*, 1994]) on the Owens Valley fault and the estimate (6.9±1.6 mm yr^{-1}) in Table 2 calls into question the validity of representing deformation in the ECSZ solely by slip at depth on the three principal fault systems there. Although *Beanland and Clark* [1994] admit some uncertainty in the geologic estimate of the slip rate on the Owens Valley fault, their arguments for a low slip rate are convincing. For example, the 6.9±1.6 mm yr^{-1} slip rate proposed here would require an earthquake similar to the 1872 Owens Valley event roughly every 1000 years, whereas the geologic evidence suggests only three such earthquakes in the last 10,000 to 20,000 years [*Beanland and Clark*, 1994]. *Dixon et al.* [2000] suggest that the current high slip rate on the Owens Valley fault inferred from GPS might be explained by postseismic relaxation following the 1872 earthquake. The slip rate in the later part of the earthquake cycle would be expected to be much less, so that the slip rate averaged over the entire interseismic interval could approach 2 mm yr^{-1}.

5. Discussion

Hearn and Humphreys [1998] modeled the deformation across the Eastern California Shear Zone using geologic slip rates and the sparse geodetic data then available. They divided the region into fault blocks using the major fault systems as boundaries and then, subject to constraints imposed by the geodetic and geologic observations, determined the slip rates on those faults which minimized the elastic energy accumulation. Their model M2 represents the best approximation to block motion consistent with the data. Because *Hearn and Humphreys* [1998] model the block motion (i.e., motion averaged over many earthquake cycles) whereas we observe the interseismic deformation, direct comparison of of their model with our observations is not possible. However, the observed motions of the rigid blocks on either side of the ECSZ are generally consistent with model M2. For example, their model M2 predicts 12.7±1.5 mm yr^{-1}

Table 2. Slip Rates Estimated from GPS Measurements for Fault Systems within the Eastern California Shear Zone

Fault System	R.-L. Slip Rate, mm yr^{-1}
Death Valley-Furnace Cr.-S. Death Valley	3.2±0.9
Hunter Mountain-Panamint Valley	3.3±1.6
Owens Valley-Little Lake	6.9±1.6

Quoted uncertainties are standard deviations

N50°±5°W for the velocity of the Sierra Nevada block and 2.5 mm yr^{-1} N87°W for the velocity of the southern Nevada plate, whereas our observed velocity on the Sierra Nevada plate (monument 3187) is 13.9±1.4 mm yr^{-1} N39°±6°W and the average velocity for the stations in the Nevada subarray is 3.0 mm yr^{-1} N71°W. In distributing slip within the ECSZ model M2 requires a 1.5-2.3 mm yr^{-1} right-lateral slip rate on the Owens Valley-Little Lake fault system (in good agreement with the geologic estimate of *Beanland and Clark* [1994]) and a 5-6 mm yr^{-1} right-lateral slip rate on the Death Valley-Furnace Creek-Southern Death Valley fault system, whereas we infer (Table 2) 6.9±1.6 mm yr^{-1} on the former fault system and 3.2±0.9 mm yr^{-1} on the latter. The agreement is better for the Hunter Mountain-Panamint fault system (model M2 predicts 2-3 mm yr^{-1} right-lateral slip whereas we infer 3.3±1.6 mm yr^{-1}). In summary our observations are consistent with the overall pattern of deformation predicted by *Hearn and Humphreys* [1998] but differ in the detailed distribution of slip inside the ECSZ where our observations suggest deformation is concentrated more to the west side of the shear zone (Owens Valley-Little Lake fault system) and model M2 indicates that the deformation is concentrated on the east side (Death Valley-Furnace Creek-Southern Death Valley fault system).

Distributed shear such as we have observed in the ECSZ is generally associated with ductile flow. However, because the upper crust itself is thought to be brittle, ductile flow there is not a viable explanation of the observed distributed deformation. Rather, the deformation must be attributed to elastic deformation in the upper crust that occurs in response to deformation in the lower crust and upper mantle. Two explanations are available for the observed concentration of strain accumulation along plate boundaries. The explanations are based on different assessments of the relative strengths of the upper crust and the upper mantle.

The conventional model (Figure 5a) assumes that the strength of the lithosphere resides principally in the upper crust; that is, the upper crust acts as a stress guide. A shear zone at the surface is then interpreted as the consequence of elastic strain accumulation due to slip at depth on a fault [*Savage and Burford*, 1973]. For example, consider a transform boundary. In the absence of a plate boundary fault, the contacting plates would both be uniformly strained. However, where a transform fault exists at the plate boundary, the relative motion of the plates is accommodated by slip at depth on the fault, with only the uppermost 10 to 20 km of the fault locked. This flaw (a slipping fault at depth) causes the surface strain accumulation to concentrate along the fault with negligible strain accumulation beyond a horizontal distance of more than about six locking depths from the fault; hence the appearance of a shear zone at the surface.

Alternatively, one may argue [*England and Jackson*, 1989; *Bourne et al.*, 1998] that the strength of the lithosphere resides primarily in the upper mantle. The upper crust is then regarded as a badly fractured layer that passively follows the deformation of the underlying upper mantle, which is undergoing ductile flow. A shear zone (Figure 5b) observed at the surface is regarded simply as elastic deformation driven by basal tractions exerted upon the upper crust by ductile flow in the upper mantle, presumably flow concentrated at a zone of weakness at the plate boundary (shear zone in upper mantle). The weak upper crust above is dragged along by the deformation of the upper mantle. This viewpoint is represented in the thin viscous sheet model of deformation [*England and Jackson*, 1989], where the entire lithosphere is modeled by a thin viscous layer. The elastic strain imposed upon the upper crust is eventually relieved by rupture on faults so that in the long term the upper crust deforms by block motion.

Our observations across the ECSZ suggest that deformation is relatively uniform across the shear zone, not clearly concentrated upon the principal faults in the zone. This would appear to favor the hypothesis that the deformation is imposed by a shear zone at depth in the upper mantle. However, if reasonable locking depths are assigned to the principal faults within the ECSZ and slip rates for those faults selected to be as consistent with the observed deformation as possible, the deformation at the surface of the shear zone is relatively uniform (Figure 4). However, the slip rate assigned to the Owens Valley fault in this model is not in agreement with the secular slip rate inferred from geology.

6. Conclusions

To a first approximation deformation across the ECSZ can be attributed to distributed uniform simple shear across vertical planes parallel to the tangent to the local small circle drawn about the North America-Pacific pole of rotation. However, the observations imply a marginally significant extension rate $\dot{\varepsilon}_{22}$= 18.2±7.2 nstrain yr^{-1} parallel to the shear direction (N36°W) that is not explained by the model. A better solution is to resolve the strain rates into a coordinate system with the 2 axis parallel to the trend of the ECSZ (N23°W). In that coordinate system the deformation corresponds to simple right-lateral shear $\dot{\varepsilon}'_{12}$= -39.2±4.4 nstrain yr^{-1} across a vertical plane striking parallel to the shear zone plus an extension, $\dot{\varepsilon}'_{11}$= 24.9±6.5 nstrain yr^{-1} perpendicular to the trend of the zone, with no significant extension $\dot{\varepsilon}'_{22}$ parallel to the zone. This corresponds to the flat-Earth deformation zone model of *Savage et al.* [1995, appendix] in which the Sierra Nevada block is translating both parallel to the Eastern California Shear Zone and away from it relative to the southern Nevada block (Figure 5b). In that model the motion is accommodated by uniform extension and shear within the ECSZ, and the Sierra block does not rotate to accommodate a fan-like opening of the Basin and Range province. The deformation can also be attributed to slip at depth on the principal fault systems within the ECSZ (Figures 4 and 5a and Table 2). However, such an explanation requires a slip rate on the Owens Valley fault at least 3 times greater than that inferred from geology [*Beanland and Clark*, 1994], a discrepancy which calls into question the validity of the model.

Acknowledgment. We thank Danan Dong for his assistance in using his adjustment program QOCA.

References

Beanland, S., and M.M. Clark, The Owens Valley Fault Zone, eastern California, and surface rupture associated with the 1872 earthquake, *U.S. Geol. Surv. Bull., 1982*, 29 pp., 1994.

Bennett, R.A., B.P. Wernicke, J.L. Davis, P Elosegui, J.K. Snow, M. J. Abolins, M.A. House, G.L. Stirewalt, and D.A. Ferrill, Global Positioning System constraints on fault slip rates in the Death Valley region, California and Nevada, *Geophys. Res. Lett., 24*, 3073-3076, 1997.

Bhattacharyya, J., S. Gross, J. Lees, and M. Hastings, Recent earthquake sequences at Coso: Evidence for conjugate faulting and stress loading near a geothermal field, *Bull. Seismol. Soc. Am., 89*, 785-795, 1999.

Bogen, N.L., and R.A. Schweickert, Magnitude of crustal extension across the northern Basin and Range province: Constraints from paleomagnetism, *Earth Planet. Sci. Lette, 75*, 93-100, 1985.

Bourne, S.J., P.C. England, and B. Parsons, The motion of crustal blocks driven by flow of the lower lithosphere: Implications for slip rates of faults in the South Island of New Zealand and southern California, *Nature, 391*, 655-659, 1998.

DeMets, C., R.G. Gordon, D.F. Argus, and S. Stein, Current plate motions, *Geophys. J. Int., 101*, 425-478, 1990.

Dixon, T.H., M. Miller, F. Farina, H. Wang, and D. Johnson, Present-day motion of the Sierra block and some tectonic implications for the Basin and Range province, North America Cordillera, *Tectonics, 24*, 1-24, 2000.

Dokka, R.K., and C.J. Travis, Late Cenozoic strike-slip faulting in the Mojave Desert, Califonia, *Tectonics, 9*, 311-340, 1990a.

Dokka, R.K. and C.J. Travis, Role of the eastern California shear zone in accommodating Pacific-North American plate motion, *Geophys. Res. Lett., 17*, 1323-1326, 1990b.

Dong, D., T.A. Herring, and R.W. King, Estimating regional deformation from a combination of space and terrestrial geodetic data, *J. Geod., 72*, 200-214, 1998.

England, P., and J. Jackson, Active deformation of the continents, *Anu. Rev. Earth Planet. Sci., 17*, 197-226, 1989.

Hearn, E.H., and E.D. Humphreys, Kinematics of the southern Walker Lane belt and motion of the Sierra Nevada block, California, *J. Geophys. Res., 103*, 27,033-27,049, 1998.

McClusky, S., S. Bjornstad, B. Hager, E. Hearn, R. King, B. Meade, M. Miller, F. Monastero, and B. Souter, Geodetic constraints on deformation in the southern Walker Lane Belt, California (abstract), in *Proceedings and Abstracts, 1999 SCEC Annual Meeting*, p. 81, South, Calif. Earthquake Cent., Univ. of South. Calif., Los Angeles, 1999.

Okada, Y., Surface deformation due to shear and tensile faults in a half-space, *Bull. Seismol. Soc. Am., 75*, 1135-1154, 1985.

Savage, J.C., and R.O. Burford, Geodetic determination of relative plate motion in central California, *J. Geophys. Res., 78*, 832-843, 1973.

Savage, J.C., and M. Lisowski, Strain accumulation in Owens Valley, California, 1974-1988, *Bull Seismol. Soc. Am., 85*, 151-158, 1995.

Savage, J.C., M. Lisowski, J.L. Svarc, and W.K. Gross, Strain accumulation across the central Nevada seismic zone, 1973-1994, *J. Geophys. Res., 100*, 20,257-20269, 1995.

Savage, J.C., J.L. Svarc, and W.H. Prescott, Geodetic estimates of fault slip rates in the San Francisco Bay area, *J. Geophys. Res., 104*, 4995-5002, 1999a.

Savage, J.C., J.L. Svarc, and W.H. Prescott, Strain accumulation at Yucca Mountain, Nevada, 1983-1998, *J. Geophys. Res., 104*, 17,627-17,631, 1999b.

Savage, J.C., J.L. Svarc, W.H. Prescott, and M.H. Murray, Deformation across the forearc of the Cascadia subduction zone at Cape Blanco, Oregon, *J. Geophys. Res., 105*, 3095-3102, 2000.

Sillard, P., Z. Altamimi, and C. Boucher, The ITRF96 realization and its associated velocity field, *Geophys. Res. Lett., 25*, 3223-3226, 1998.

Webb, F. H., and J.F. Zumberge, An introduction to GIPSY/OASIS-II, Rep. JPL D-11088, Jet Propul. Lab., Calif. Inst. of Technol., Pasadena, 1995.

Wernicke, B., J.L. Davis, R.A. Bennett, P. Elosegui, M.J. Abolins, R.J. Brady, M.A. House, N.A. Niemi, and J.K. Snow, Anomalous strain accumulation in the Yucca Mountain area, Nevada, *Science, 279*, 2096-2100, 1998.

Wicks, C.W., W. Thatcher, F.C. Monastero, and M. Hastings, Deformation of the Coso Range, east-central California, from satellite radar interferometry (abstract), *Eos Trans. AGU, 80*(46), Fall Meet. Suppl., F1194, 1999.

Zhang, J., Y. Bock, H. Johnson, P. Fang, J. Genrich, S. Williams, S. Wdowinski, and J. Behr, Southern California permanent GPS geodetic array: Error analysis of daily position estimates and site velocities, *J. Geophys. Res., 102*, 18,035-18,055, 1997.

Zumberge, J.F., M.B. Heflin, D.C. Jefferson, M.M. Watkins, and F.H. Webb, Precise point positioning for the efficient and robust analysis of GPS data from large networks, *J. Geophys. Res., 102*, 5005-5017, 1997.

W. Gan, W. H. Prescott, J. C. Savage, and J. L. Svarc, U.S. Geological Survey, MS/977, 345 Middlefield Rd, Menlo Park, CA 94025. (wjgan@usgs.gov)

(Received October 18, 1999; revised March 9, 2000;
accepted March 24, 2000)